Preprints of the 21st IFAC World Congress (Virtual)
Berlin, Germany, July 12-17, 2020

An Integrated Approach for Experimental Design, Control, and Optimization of Perfusion Bioreactors ⋆

Diogo Rodrigues *

* *Division of Decision and Control Systems, KTH Royal Institute of Technology, SE-100 44 Stockholm, Sweden (diogor@kth.se)*

Abstract: This paper presents methods for experimental design, control, and optimization of perfusion bioreactors as well as the vision for their integration. After describing a generic model of perfusion bioreactors, the paper proposes a control scheme via rate estimation and feedback linearization with useful properties with respect to steady-state error, stability, and performance. The paper also introduces data-driven and hybrid procedures for experimental design that are tailored to the intended use of the model for steady-state optimization. Lastly, the methods are illustrated via a simulation example of a perfusion bioreactor.

Keywords: model, experimental design, control, optimization, perfusion, bioreactors

1. INTRODUCTION

Continuous manufacturing has been indicated as an economically optimal mode of operation for production of biologics such as monoclonal antibodies. On the other hand, it is more difficult to operate it so as to ensure reproducibility and facilitate process validation (Pollock et al., 2013). One of the key components in such a process is the production of biologics via animal cell culture in perfusion bioreactors. In these reactors, the cell culture remains in the reactor owing to a cell retention device and the product of interest is continuously harvested. Previous experimental work has shown a very high viable cell density and a cell-specific productivity comparable to fed-batch reactors in perfusion bioreactors coupled to alternating tangential flow systems (Clincke et al., 2013). The improvement of the cell-specific productivity is the object of ongoing work since it highly depends on the cell line and product of interest.

For this purpose, mathematical modeling and model-based control and optimization are proposed as alternatives to the exhaustive screening of culture media that is still the industrial practice (Chotteau, 2015). However, there is no consensus regarding the most appropriate procedures for model identification, experimental design, and use of the resulting mathematical model for control and optimization in the context of perfusion bioreactors. This paper attempts to deal with these challenges via an integrated approach that encompasses procedures for experimental design, control, and optimization of perfusion bioreactors.

The dynamic models used for control of processes such as perfusion bioreactors are typically incomplete. The concept of rate estimation can be used to estimate the unknown part of the incomplete model without identifying its model. This concept has already been developed and applied to control of continuous reactors (Rodrigues et al., 2018), using an approach for control design via feedback linearization (Farschman et al., 1998). This paper recalls the control strategy via rate estimation and feedback linearization proposed and analyzed by Rodrigues and Hjalmarsson (2019) and applies it to perfusion bioreactors.

One of the goals of this paper is the development of procedures for mathematical modeling and experimental design of perfusion bioreactors for use of the resulting model to optimize the steady-state operation of perfusion bioreactors. Hence, it makes sense to tailor the procedure for experimental design to this intended goal. This idea is in line with the notion advocated in the literature that process models and the experiments performed to identify these models should be tailored to their purpose, which is steady-state optimization of perfusion bioreactors in this study (Bonvin et al., 2016). For this reason, this paper shows how one can design experiments to model for optimization.

The paper presents the generic model of perfusion bioreactors and the multivariable control structure that deals with the fact that perfusion bioreactors are typically described by incomplete models. In addition, it introduces two algorithms for experimental design that can be used to identify models that are adequate for their intended purpose.

2. MODEL OF PERFUSION BIOREACTORS

In perfusion bioreactors, suspended cells are cultivated in a liquid medium that is continuously renewed via the inlets and outlets. The goal is to make the cells generate a certain product of interest and to recover that product continuously. To avoid loss of productivity due to dilution of biomass and to facilitate downstream processing, perfusion bioreactors are coupled to a cell retention device. This ensures that the biomass remains in the reactor and the other extracellular species, including the product of interest, are continuously harvested. Moreover, a so-called bleed stream is typically used to avoid accumulation of dead cells.

Hence, a perfusion bioreactor is a constant-volume, continuous, agitated bioreactor that is intended to operate predominantly at steady state, but here its transient behavior is shown as a dynamic model. In this biological reaction

⋆ This work was supported by the VINNOVA Competence Centre AdBIOPRO, contract 2016-05181.

system with R reactions and S species and described by the stoichiometric matrix $\mathbf{N}$ of dimension $R \times S$, there are S_{ec} extracellular species and S_{ic} intracellular species. These species are selected using the selection matrices $\mathbf{S}_{ec}$ of dimension $S_{ec} \times S$ and $\mathbf{S}_{ic}$ of dimension $S_{ic} \times S$, respectively. The stoichiometries of the reactions that affect the intracellular and extracellular species are given by the matrices $\mathbf{N}_{ic} = \mathbf{N}\mathbf{S}_{ic}^{\mathrm{T}}$ and $\mathbf{N}_{ec} = \mathbf{N}\mathbf{S}_{ec}^{\mathrm{T}}$, respectively. For these systems, a pseudo steady-state assumption for the intracellular species is typically used. This means that the generic dynamic model of a perfusion bioreactor is described by the following system of differential-algebraic equations:

$$\dot{\mathbf{c}}(t) = \mathbf{N}_{ec}^{\mathrm{T}}\mathbf{r}_c\big(\mathbf{c}(t)\big) + \mathbf{C}_{in}(t)\boldsymbol{\omega}_{in}(t) - \boldsymbol{\Omega}(t)\mathbf{c}(t), \tag{1a}$$

$$\mathbf{0}_{S_{ic}} = \mathbf{N}_{ic}^{\mathrm{T}}\mathbf{r}_c\big(\mathbf{c}(t)\big), \tag{1b}$$

where $\mathbf{c}(t)$ is the S_{ec}-dimensional vector of bioreactor concentrations of extracellular species including biomass in moles per unit of volume, $\boldsymbol{\omega}_{in}(t)$ is the p-dimensional vector of inlet rates in reactor volumes per unit of time, $\mathbf{C}_{in}(t)$ is the $S_{ec} \times p$ matrix of inlet concentrations of extracellular species including biomass, $\boldsymbol{\Omega}(t) := \omega_p(t)\mathbf{I}_{S_{ec}} - \omega_h(t)\mathbf{R}(t)$, $\mathbf{R}(t)$ is the S_{ec}-dimensional diagonal matrix of retention factors for the extracellular species, and $\omega_p(t)$ is the perfusion rate in reactor volumes per unit of time, which corresponds not only to the sum of the harvest rate $\omega_h(t)$ and bleed rate $\omega_b(t)$ but also to the sum of inlet rates $\boldsymbol{\omega}_{in}(t)$, that is, $\mathbf{1}_p^{\mathrm{T}}\boldsymbol{\omega}_{in}(t) = \omega_p(t) = \omega_h(t) + \omega_b(t)$. Furthermore, $\mathbf{r}_c\big(\mathbf{c}(t)\big)$ are reaction rates per unit of volume per unit of time, and their dependence on the concentrations is typically the only unknown part of the model, which needs to be estimated from experiments via appropriate model identification techniques. Also, $\mathbf{r}(t) = \frac{\mathbf{r}_c(\mathbf{c}(t))}{VC(t)}$ are specific reaction rates per cell per unit of time, shown without the dependence on the concentrations, where $VC(t)$ is the viable cell concentration in viable cells per unit of volume.

In the case of biomass, $c_{biom}(t) = f_{biom}VC(t)$ is its concentration in moles per unit of volume, where f_{biom} is a scaling factor. Biomass is selected from the extracellular species using the S_{ec}-dimensional selection vector $\mathbf{s}_{biom}$ such that $c_{biom}(t) = \mathbf{s}_{biom}^{\mathrm{T}}\mathbf{c}(t)$, the stoichiometries of the reactions that affect it are given by the vector $\mathbf{n}_{biom} = \mathbf{N}_{ec}\mathbf{s}_{biom}$, its retention factor is $R_{biom}(t) = \mathbf{s}_{biom}^{\mathrm{T}}\mathbf{R}(t)\mathbf{s}_{biom} = 1$, and its p-dimensional row vector of inlet concentrations is $\mathbf{c}_{in,biom}(t) = \mathbf{s}_{biom}^{\mathrm{T}}\mathbf{C}_{in}(t) = \mathbf{0}_p^{\mathrm{T}}$, which implies that

$$\dot{c}_{biom}(t) = \mathbf{n}_{biom}^{\mathrm{T}}\mathbf{r}_c\big(\mathbf{c}(t)\big) - \omega_b(t)c_{biom}(t). \tag{2}$$

One can also model the perfusion bioreactor in terms of flux modes (FMs). Let R_m denote the number of FMs, and let $\mathbf{N}_m$ of dimension $R_m \times S$ and rank R_m denote the matrix of stoichiometries of the FMs. Once $\mathbf{N}_m$ is chosen, one can know which linear combinations of the stoichiometries in the rows of $\mathbf{N}$ correspond to the stoichiometries of the FMs in the rows of $\mathbf{N}_m$. In other words, one can compute the $R \times R_m$ matrix $\mathbf{E}_m$ of rank R_m such that $\mathbf{N}^{\mathrm{T}}\mathbf{E}_m = \mathbf{N}_m^{\mathrm{T}}$.

One can show that the true reaction system can always be described correctly by using the stoichiometry of the FMs represented by a particular $\mathbf{N}_m$ since there exists some R_m-dimensional vector of rates $\boldsymbol{\psi}(t)$ such that $\mathbf{r}(t) = \mathbf{E}_m\boldsymbol{\psi}(t)$.

The remarks above and the fact that $\boldsymbol{\psi}_c\big(\mathbf{c}(t)\big)$ are reaction rates for the FMs per unit of volume per unit of time imply that the model (1) can be equivalently written as

$$\dot{\mathbf{c}}(t) = \mathbf{N}_{ec}^{\mathrm{T}}\mathbf{E}_m\boldsymbol{\psi}_c\big(\mathbf{c}(t)\big) + \mathbf{C}_{in}(t)\boldsymbol{\omega}_{in}(t) - \boldsymbol{\Omega}(t)\mathbf{c}(t), \tag{3}$$

while $\boldsymbol{\psi}(t) = \frac{\boldsymbol{\psi}_c(\mathbf{c}(t))}{VC(t)}$ are specific reaction rates for the FMs per cell per unit of time, shown without the dependence on the concentrations. In the case of biomass, it is known that

$$\dot{c}_{biom}(t) = \mathbf{n}_{biom}^{\mathrm{T}}\mathbf{E}_m\boldsymbol{\psi}_c\big(\mathbf{c}(t)\big) - \omega_b(t)c_{biom}(t). \tag{4}$$

Also, S_a extracellular species with concentrations $\mathbf{c}_a(t)$ are measured and correspond to the $S_a \times S$ selection matrix $\mathbf{S}_a$ and the stoichiometric matrix $\mathbf{N}_a = \mathbf{N}\mathbf{S}_a^{\mathrm{T}}$.

3. CONTROL BASED ON INCOMPLETE MODELS

System identification can be used to obtain a relatively accurate description of the dynamic model of perfusion bioreactors. However, this description remains subject to some imprecision and requires experimental work that may be time-consuming and expensive. Hence, the goal of this section is to present a multivariable control structure that deals with the fact that the models of perfusion bioreactors may be incomplete and not only is simple to tune and understand but also ensures good closed-loop performance.

Although a previous conference paper has already presented most of the strategy for generic systems (Rodrigues and Hjalmarsson, 2019), this section applies this method to the particular case of perfusion bioreactors, where typically the goal is to control the S_c linear combinations of outputs $\mathbf{c}_c(t) := \mathbf{S}_c\mathbf{c}_a(t)$ to the setpoints $\mathbf{c}_c^s(t)$ by measuring the outputs $\mathbf{c}_a(t)$ and manipulating the inputs $\boldsymbol{\omega}_{in}(t)$.

3.1 Problem description

Consider the nonlinear system that corresponds to a perfusion bioreactor with $n_x := S_{ec}$ states $\mathbf{x}(t) := \mathbf{c}(t)$, $n_u := p$ inputs $\mathbf{u}(t) := \boldsymbol{\omega}_{in}(t)$, and $n_y := S_a$ outputs $\mathbf{y}(t) := \mathbf{c}_a(t)$. The state dynamics are composed of an unknown part and a known or available part, denoted by subscripts u and a, and the outputs are known linear combinations of the states. The dynamic model is written as:

$$\dot{\mathbf{x}}(t) = \mathbf{f}_u\big(\mathbf{x}(t), \mathbf{u}(t)\big) + \mathbf{f}_a\big(\mathbf{x}(t), \mathbf{u}(t)\big), \quad \mathbf{x}(0) = \mathbf{x}_0, \tag{5a}$$

$$\mathbf{y}(t) = \mathbf{C}\mathbf{x}(t), \tag{5b}$$

where $\mathbf{f}_a\big(\mathbf{x}(t), \mathbf{u}(t)\big) := \mathbf{C}_{in}(t)\boldsymbol{\omega}_{in}(t) - \boldsymbol{\Omega}(t)\mathbf{c}(t)$ is a known function, $\mathbf{f}_u\big(\mathbf{x}(t), \mathbf{u}(t)\big) := \mathbf{N}_{ec}^{\mathrm{T}}\mathbf{E}_m\boldsymbol{\psi}_c\big(\mathbf{c}(t)\big)$ is an unknown function, and $\mathbf{C} := \mathbf{S}_a\mathbf{S}_{ec}^{\mathrm{T}}$ is a known matrix. In addition, (i) $\mathbf{s}_a\big(\mathbf{y}(t), \mathbf{u}(t)\big) := \mathbf{C}\mathbf{f}_a\big(\mathbf{x}(t), \mathbf{u}(t)\big) = \mathbf{S}_a\mathbf{S}_{ec}^{\mathrm{T}}\mathbf{C}_{in}(t)\boldsymbol{\omega}_{in}(t) - \boldsymbol{\Omega}_a(t)\mathbf{c}_a(t)$ can be computed from the current outputs and inputs, and (ii) $\mathbf{s}_u\big(\mathbf{x}(t)\big) := \mathbf{C}\mathbf{f}_u\big(\mathbf{x}(t), \mathbf{u}(t)\big) = \mathbf{S}_a\mathbf{N}_m^{\mathrm{T}}\boldsymbol{\psi}_c\big(\mathbf{c}(t)\big)$ is an unknown function of the states only.

Assuming that $\mathbf{S}_a\mathbf{N}_m^{\mathrm{T}}$ is of full column rank R_m, one writes $\mathbf{s}_u\big(\mathbf{x}(t)\big)$ as linear combinations of $n_r := R_m$ rates $\mathbf{r}_u\big(\mathbf{x}(t)\big) := \boldsymbol{\psi}_c\big(\mathbf{c}(t)\big)$, that is, $\mathbf{s}_u\big(\mathbf{x}(t)\big) = \boldsymbol{\mathcal{L}}\mathbf{r}_u\big(\mathbf{x}(t)\big)$, where $\mathbf{r}_u\big(\mathbf{x}(t)\big)$ is an unknown function and $\boldsymbol{\mathcal{L}} := \mathbf{S}_a\mathbf{N}_m^{\mathrm{T}}$ is a known $n_y \times n_r$ matrix with rank n_r, which implies $n_r \leq n_y$ and there is an $n_r \times n_y$ matrix $\boldsymbol{\mathcal{T}}$ such that $\boldsymbol{\mathcal{T}}\boldsymbol{\mathcal{L}} = \mathbf{I}_{n_r}$.

Hence, one defines the n_r states $\mathbf{x}_r(t) := \boldsymbol{\mathcal{T}}\mathbf{C}\mathbf{c}(t)$ and the outputs $\mathbf{y}_r(t) := \boldsymbol{\mathcal{T}}\mathbf{c}_a(t)$ described by the dynamics

$$\dot{\mathbf{x}}_r(t) = \mathbf{r}_u\big(\mathbf{x}(t)\big) + \boldsymbol{\mathcal{T}}\mathbf{s}_a\big(\mathbf{y}(t), \mathbf{u}(t)\big), \quad \mathbf{x}_r(0) = \mathbf{x}_{r,0}, \tag{6a}$$

$$\mathbf{y}_r(t) = \mathbf{x}_r(t). \tag{6b}$$

Suppose that the objective is to control the $n_c := S_c$ linear combinations of outputs $\mathbf{y}_c(t) := \mathbf{c}_c(t)$ to the setpoints $\mathbf{y}_c^s(t) := \mathbf{c}_c^s(t)$. These linear combinations are given by the

$n_c \times n_y$ matrix $\mathbf{S} := \mathbf{S}_c$ with rank n_c, which implies $n_c \leq n_y$. Hence, one defines the n_c states $\mathbf{x}_c(t) := \mathbf{SC}\mathbf{c}(t)$ and the outputs $\mathbf{y}_c(t) := \mathbf{c}_c(t)$ described by the dynamics

$$\dot{\mathbf{x}}_c(t) = \mathbf{H}\mathbf{r}_u\big(\mathbf{x}(t)\big) + \mathbf{h}_a\big(\mathbf{y}(t), \mathbf{u}(t)\big), \quad \mathbf{x}_c(0) = \mathbf{x}_{c,0}, \tag{7a}$$

$$\mathbf{y}_c(t) = \mathbf{x}_c(t), \tag{7b}$$

where $\mathbf{H} := \mathbf{S}_c\mathbf{S}_a\mathbf{N}_m^{\mathrm{T}}$ and $\mathbf{h}_a\big(\mathbf{y}(t), \mathbf{u}(t)\big) = \mathbf{B}_a\big(\mathbf{y}(t)\big)\mathbf{u}(t) + \boldsymbol{\beta}_a\big(\mathbf{y}(t)\big)$, with $\boldsymbol{\beta}_a\big(\mathbf{y}(t)\big) := -\boldsymbol{\Omega}_c(t)\mathbf{c}_c(t)$ and $\mathbf{B}_a\big(\mathbf{y}(t)\big) := \mathbf{S}_c\mathbf{S}_a\mathbf{S}_{ec}^{\mathrm{T}}\mathbf{C}_{in}(t)$.

3.2 Control strategy

Unfortunately, the rate model $\mathbf{r}_u\big(\mathbf{x}(t)\big) := \boldsymbol{\psi}_c\big(\mathbf{c}(t)\big)$ is unknown and there is a difference between the system inputs $\mathbf{u}(t) := \boldsymbol{\omega}_{in}(t)$ and the actuator inputs $\tilde{\mathbf{u}}(t) := \tilde{\boldsymbol{\omega}}_{in}(t)$ due to the input disturbances $\mathbf{d}(t) := \mathbf{u}(t) - \tilde{\mathbf{u}}(t)$ and a difference between the sensor outputs $\tilde{\mathbf{y}}(t) := \tilde{\mathbf{c}}_a(t)$ and the system outputs $\mathbf{y}(t) := \mathbf{c}_a(t)$ due to the output disturbances $\mathbf{w}(t) := \tilde{\mathbf{y}}(t) - \mathbf{y}(t)$. However, one can deal with these issues as shown below.

If the matrix $\mathbf{B}_a\big(\tilde{\mathbf{y}}(t)\big)$ is invertible, which implies $n_c = n_u$ and is typically true for the proposed choice of controlled outputs $\mathbf{y}_c(t)$, one can use the feedback linearization law

$$\tilde{\mathbf{u}}(t) = \mathbf{B}_a\big(\tilde{\mathbf{y}}(t)\big)^{-1}\Big(\mathbf{v}(t) - \mathbf{H}\hat{\mathbf{r}}_u(t) - \boldsymbol{\beta}_a\big(\tilde{\mathbf{y}}(t)\big)\Big). \tag{8}$$

For the rates of variation $\mathbf{v}(t)$, one can choose among other alternatives the proportional control law with gain τ_c^{-1}

$$\mathbf{v}(t) = \tau_c^{-1}\big(\mathbf{y}_c^s(t) - \tilde{\mathbf{y}}_c(t)\big), \tag{9}$$

which would ensure exponential convergence of $\mathbf{y}_c(t)$ to $\mathbf{y}_c^s(t)$ with the time constant τ_c in the ideal case of known rate model $\mathbf{r}_u\big(\mathbf{x}(t)\big)$ and no input and output disturbances.

Several options exist for estimation of the rates $\mathbf{r}_u\big(\mathbf{x}(t)\big)$, for example sliding mode observers (Nuñez et al., 2013). Here, the finite impulse response filter proposed by Rodrigues and Hjalmarsson (2019) is adopted since the resulting rate estimates $\hat{\mathbf{r}}_u(t)$ consist of the effect of $\mathbf{w}$ and a weighted average of $\mathbf{r}_u$ in $[t - \Delta t, t]$, where Δt is the size of the filter window. The values $\hat{\mathbf{r}}_u(t)$ of the unknown rate signals are estimated from the measured signals $\tilde{\mathbf{y}}_r(t) := \boldsymbol{\mathcal{T}}\tilde{\mathbf{y}}(t)$ and the available rates $\tilde{\mathbf{s}}_a(t)$ computed from $\tilde{\mathbf{y}}(t)$ and $\tilde{\mathbf{u}}(t)$:

$$\hat{\mathbf{r}}_u(t) = \int_0^{\Delta t}\Big(\tfrac{c(\tau)}{\Delta t^2}\tilde{\mathbf{y}}_r(t-\Delta t+\tau) - \tfrac{b(\tau)}{\Delta t}\boldsymbol{\mathcal{T}}\tilde{\mathbf{s}}_a(t-\Delta t+\tau)\Big)\,\mathrm{d}\tau, \tag{10}$$

where $c(\tau)$ and $b(\tau)$ are convolution functions. For the sake of brevity, all the signals are presented as functions of time.

Under the assumptions stated by Rodrigues and Hjalmarsson (2019), one can show that the functions $c(\tau)$ and $b(\tau)$ that minimize the effect of measurement noise in $\mathbf{w}(t)$ are

$$c(\tau) = 12\tfrac{\tau}{\Delta t} - 6, \tag{11a}$$

$$b(\tau) = -6\left(\tfrac{\tau}{\Delta t}\right)^2 + 6\tfrac{\tau}{\Delta t}, \tag{11b}$$

with the matrix $\boldsymbol{\mathcal{T}} = \big(\boldsymbol{\mathcal{L}}^{\mathrm{T}}\boldsymbol{\Sigma}_{\mathbf{w}}^{-1}\boldsymbol{\mathcal{L}}\big)^{-1}\boldsymbol{\mathcal{L}}^{\mathrm{T}}\boldsymbol{\Sigma}_{\mathbf{w}}^{-1}$, where $\boldsymbol{\Sigma}_{\mathbf{w}}$ is the covariance matrix of the noise in $\mathbf{w}(t)$.

The presented control strategy requires only two design parameters with a well-defined meaning: (i) Δt is the window size of the differentiation filter, which should be small enough so that the unknown rates $\mathbf{r}_u\big(\mathbf{x}(t)\big)$ are approximately constant in this window, but not too small to prevent amplification of measurement noise; and (ii) τ_c is the inverse of the controller gain and is expected to be approximately equal to the dominant closed-loop time constant if the rate estimation is accurate enough.

3.3 Stability and performance

The conference paper by Rodrigues and Hjalmarsson (2019) provided a method to perform stability and performance analysis for this control strategy. One can also show that the closed-loop system eliminates the steady-state error.

In that paper, an example of a continuous stirred-tank (nonisothermal) reactor with 4 species and 2 reactions was presented. This system is described by a model with 5 states, 3 inputs, and 3 (controlled) outputs, the heat and the numbers of moles of 2 species. The response of the closed-loop system to step increases in the setpoints showed that the controlled outputs converge to the new setpoint values rather quickly, which means that no steady-state error is present. Furthermore, it was shown that the closed-loop performance becomes worse with increasing values of τ_c and Δt, but the stability is not compromised.

Although the model of this example includes fewer states, inputs, and outputs than the model of a typical perfusion bioreactor, the models are similar, which allows drawing conclusions about the stability and performance of the control strategy for perfusion bioreactors from this example.

4. DESIGN OF EXPERIMENTS FOR OPTIMIZATION

One would like to tailor the procedure for experimental design to the intended goal, that is, optimization of the steady-state operation of perfusion bioreactors. This task is simplified by a control strategy such as the one in the previous section, which deals with the manipulation of the inputs that is necessary for the controlled outputs to reach certain setpoints at steady state and allows reducing the degrees of freedom to the steady-state setpoints. Hence, in this section, the focus is on designing experiments to identify models that are adequate for optimization, that is, to model for optimization. More precisely, the resulting model should provide a solution to an optimization problem with some steady-state setpoints as decision variables and cost and constraints that depend on steady-state quantities.

4.1 Modeling for optimization

Suppose that one would like to model how the n_π steady-state decision variables $\bar{\boldsymbol{\pi}}$ of a system affect its n_y steady-state attributes $\bar{\mathbf{y}}^p(\bar{\boldsymbol{\pi}})$. For a closed-loop system with no steady-state error, $\bar{\boldsymbol{\pi}}$ are some steady-state setpoints $\bar{\mathbf{y}}_c^s$ and $\bar{\mathbf{y}}^p(\bar{\boldsymbol{\pi}})$ are the steady-state inputs $\bar{\mathbf{u}}^p(\bar{\boldsymbol{\pi}})$ and uncontrolled outputs $\bar{\mathbf{y}}_n^p(\bar{\boldsymbol{\pi}})$. In the particular case of a perfusion bioreactor where the outputs $\mathbf{c}_c(t)$ are controlled to the setpoints $\mathbf{c}_c^s(t)$ by measuring the outputs $\mathbf{c}_a(t)$ and manipulating the inputs $\boldsymbol{\omega}_{in}(t)$ and the outputs $\mathbf{c}_n(t)$ are uncontrolled, one defines the steady-state setpoints $\bar{\mathbf{y}}_c^s := \bar{\mathbf{c}}_c^s$ that include the steady-state decision variables $\bar{\boldsymbol{\pi}}$, and the steady-state attributes $\bar{\mathbf{y}}^p(\bar{\boldsymbol{\pi}})$ that consist in $\bar{\boldsymbol{\omega}}_{in}^p(\bar{\boldsymbol{\pi}})$ and $\bar{\mathbf{c}}_n^p(\bar{\boldsymbol{\pi}})$ since $\bar{\mathbf{c}}_c^p(\bar{\boldsymbol{\pi}}) = \bar{\mathbf{c}}_c^s$ in the case of control with no steady-state error.

We are modeling for optimization since the purpose of the model is to find an optimum $\bar{\boldsymbol{\pi}}^*$ of the problem

$$\max_{\bar{\boldsymbol{\pi}}} \phi^p(\bar{\boldsymbol{\pi}}), \tag{12a}$$

$$\text{s.t. } \mathbf{g}^p(\bar{\boldsymbol{\pi}}) \leq \mathbf{0}_g, \tag{12b}$$

with

$$\phi^p(\bar{\boldsymbol{\pi}}) := \phi\big(\bar{\mathbf{y}}^p(\bar{\boldsymbol{\pi}}), \bar{\boldsymbol{\pi}}\big), \tag{13a}$$

$$\mathbf{g}^p(\bar{\boldsymbol{\pi}}) := \mathbf{g}\big(\bar{\mathbf{y}}^p(\bar{\boldsymbol{\pi}}), \bar{\boldsymbol{\pi}}\big), \tag{13b}$$

where $\phi(\bar{\mathbf{y}}, \bar{\boldsymbol{\pi}})$ and $\mathbf{g}(\bar{\mathbf{y}}, \bar{\boldsymbol{\pi}})$ are the objective and constraint functions that depend on the steady-state attributes and decision variables, and the superscript p refers to the plant, that is, the true experimental system, in contrast to the superscript m that will be used below to refer to the model.

Furthermore, the gradients of $\phi^p(\bar{\boldsymbol{\pi}})$ and $\mathbf{g}^p(\bar{\boldsymbol{\pi}})$ can be computed from the gradients of $\bar{\mathbf{y}}^p(\bar{\boldsymbol{\pi}})$ as follows:

$$\frac{\partial \phi^p}{\partial \bar{\boldsymbol{\pi}}}(\bar{\boldsymbol{\pi}}) = \frac{\partial \phi}{\partial \bar{\mathbf{y}}}\big(\bar{\mathbf{y}}^p(\bar{\boldsymbol{\pi}}), \bar{\boldsymbol{\pi}}\big) \frac{\partial \bar{\mathbf{y}}^p}{\partial \bar{\boldsymbol{\pi}}}(\bar{\boldsymbol{\pi}}) + \frac{\partial \phi}{\partial \bar{\boldsymbol{\pi}}}\big(\bar{\mathbf{y}}^p(\bar{\boldsymbol{\pi}}), \bar{\boldsymbol{\pi}}\big), \quad (14a)$$

$$\frac{\partial \mathbf{g}^p}{\partial \bar{\boldsymbol{\pi}}}(\bar{\boldsymbol{\pi}}) = \frac{\partial \mathbf{g}}{\partial \bar{\mathbf{y}}}\big(\bar{\mathbf{y}}^p(\bar{\boldsymbol{\pi}}), \bar{\boldsymbol{\pi}}\big) \frac{\partial \bar{\mathbf{y}}^p}{\partial \bar{\boldsymbol{\pi}}}(\bar{\boldsymbol{\pi}}) + \frac{\partial \mathbf{g}}{\partial \bar{\boldsymbol{\pi}}}\big(\bar{\mathbf{y}}^p(\bar{\boldsymbol{\pi}}), \bar{\boldsymbol{\pi}}\big). \quad (14b)$$

For the model, $\phi^m(\bar{\boldsymbol{\pi}})$ and $\mathbf{g}^m(\bar{\boldsymbol{\pi}})$ are defined as functions of the steady-state model attributes $\bar{\mathbf{y}}^m(\bar{\boldsymbol{\pi}})$ as shown for the plant in (13), and the gradients of $\phi^m(\bar{\boldsymbol{\pi}})$ and $\mathbf{g}^m(\bar{\boldsymbol{\pi}})$ can be computed from the gradients of $\bar{\mathbf{y}}^m(\bar{\boldsymbol{\pi}})$ similarly to (14), by replacing the superscript p by the superscript m. All the functions above are assumed to be differentiable.

Let $\mathbf{g}_a^p(\bar{\boldsymbol{\pi}})$ denote the g_a active constraints at $\bar{\boldsymbol{\pi}}$ such that $\mathbf{g}_a^p(\bar{\boldsymbol{\pi}}) = \mathbf{0}_{g_a}$, and assume that linear independence constraint qualification holds. From the Karush-Kuhn-Tucker (KKT) conditions, it is known that, at a plant optimum $\bar{\boldsymbol{\pi}}^{p*}$, $\mathbf{g}^p(\bar{\boldsymbol{\pi}}^{p*}) \leq \mathbf{0}_g$ and there exists $\boldsymbol{\mu} \geq \mathbf{0}_{g_a}$ such that

$$\boldsymbol{\mu}^{\mathrm{T}} \frac{\partial \mathbf{g}_a^p}{\partial \bar{\boldsymbol{\pi}}}(\bar{\boldsymbol{\pi}}^{p*}) = \frac{\partial \phi^p}{\partial \bar{\boldsymbol{\pi}}}(\bar{\boldsymbol{\pi}}^{p*}). \quad (15)$$

Hence, an adequate model for optimization $\phi^m(\bar{\boldsymbol{\pi}})$, $\mathbf{g}^m(\bar{\boldsymbol{\pi}})$ must ensure that $\mathbf{g}^m(\bar{\boldsymbol{\pi}}) \leq \mathbf{0}_g$ and there exists $\boldsymbol{\mu} \geq \mathbf{0}_{g_a}$ such that $\boldsymbol{\mu}^{\mathrm{T}} \frac{\partial \mathbf{g}_a^m}{\partial \bar{\boldsymbol{\pi}}}(\bar{\boldsymbol{\pi}}) = \frac{\partial \phi^m}{\partial \bar{\boldsymbol{\pi}}}(\bar{\boldsymbol{\pi}})$ if and only if $\bar{\boldsymbol{\pi}} = \bar{\boldsymbol{\pi}}^{p*}$. In particular, an adequate model must be such that $\mathbf{g}^m(\bar{\boldsymbol{\pi}}^{p*})$ predicts correctly $\mathbf{g}^p(\bar{\boldsymbol{\pi}}^{p*})$ and $\frac{\partial \phi^m}{\partial \bar{\boldsymbol{\pi}}}(\bar{\boldsymbol{\pi}}^{p*})$, $\frac{\partial \mathbf{g}_a^m}{\partial \bar{\boldsymbol{\pi}}}(\bar{\boldsymbol{\pi}}^{p*})$ predict correctly $\frac{\partial \phi^p}{\partial \bar{\boldsymbol{\pi}}}(\bar{\boldsymbol{\pi}}^{p*})$, $\frac{\partial \mathbf{g}_a^p}{\partial \bar{\boldsymbol{\pi}}}(\bar{\boldsymbol{\pi}}^{p*})$. For this reason, the modeling effort should focus on the location of plant optima $\bar{\boldsymbol{\pi}}^{p*}$.

4.2 Data-driven algorithm for experimental design

To obtain an adequate model for optimization, it would be helpful to have an idea about the location of plant optima $\bar{\boldsymbol{\pi}}^{p*}$. However, the purpose of the model is precisely to indicate the location of plant optima $\bar{\boldsymbol{\pi}}^{p*}$. In addition, the design of new experiments is needed because one admits that the model is poorly known or even unknown, thus not even the location of any model optimum $\bar{\boldsymbol{\pi}}^{m*}$ is known.

However, even if the model is known, gradient-based optimization algorithms face the same situation before they reach a model optimum. Hence, recall how a gradient-based optimization algorithm works and note that all its steps can be performed if the model is replaced with the experimental system. This inspires the data-driven algorithm for experimental design presented below, which uses the same steps of a gradient-based optimization algorithm and the experimental system to *design the experimental points*:

(1) Start from the *experimental point* $\bar{\boldsymbol{\pi}}_0$ and set $k = 0$.
(2) Use *experiments to measure* $\tilde{\mathbf{y}}^p(\bar{\boldsymbol{\pi}}_k)$, $\tilde{\mathbf{y}}^p(\bar{\boldsymbol{\pi}}_k^1)$, …, $\tilde{\mathbf{y}}^p(\bar{\boldsymbol{\pi}}_k^{n_\pi})$, and *estimate* $\mathbf{y}^p(\bar{\boldsymbol{\pi}}_k)$, $\frac{\partial \mathbf{y}^p}{\partial \bar{\boldsymbol{\pi}}}(\bar{\boldsymbol{\pi}}_k)$ as the solution to $\tilde{\mathbf{y}}^p(\bar{\boldsymbol{\pi}}_k^l) = \big[\mathbf{y}^p(\bar{\boldsymbol{\pi}}_k) \ \frac{\partial \mathbf{y}^p}{\partial \bar{\boldsymbol{\pi}}}(\bar{\boldsymbol{\pi}}_k)\big] \big[1 \ (\bar{\boldsymbol{\pi}}_k^l - \bar{\boldsymbol{\pi}}_k)^{\mathrm{T}}\big]^{\mathrm{T}}$, for $l = 0, 1, \ldots, n_\pi$, with $\bar{\boldsymbol{\pi}}_k^0 = \bar{\boldsymbol{\pi}}_k$.
(3) Compute $\phi^p(\bar{\boldsymbol{\pi}}_k)$, $\mathbf{g}^p(\bar{\boldsymbol{\pi}}_k)$, $\frac{\partial \phi^p}{\partial \bar{\boldsymbol{\pi}}}(\bar{\boldsymbol{\pi}}_k)$, $\frac{\partial \mathbf{g}^p}{\partial \bar{\boldsymbol{\pi}}}(\bar{\boldsymbol{\pi}}_k)$ from $\mathbf{y}^p(\bar{\boldsymbol{\pi}}_k)$, $\frac{\partial \mathbf{y}^p}{\partial \bar{\boldsymbol{\pi}}}(\bar{\boldsymbol{\pi}}_k)$ using (13) and (14).
(4) Test whether $\mathbf{g}^p(\bar{\boldsymbol{\pi}}_k) \leq \mathbf{0}_g$ and there exists $\boldsymbol{\mu} \geq \mathbf{0}_{g_a}$ such that $\boldsymbol{\mu}^{\mathrm{T}} \frac{\partial \mathbf{g}_a^p}{\partial \bar{\boldsymbol{\pi}}}(\bar{\boldsymbol{\pi}}_k) \simeq \frac{\partial \phi^p}{\partial \bar{\boldsymbol{\pi}}}(\bar{\boldsymbol{\pi}}_k)$.
If so, *end the experiments* since $\bar{\boldsymbol{\pi}}_k$ is near $\bar{\boldsymbol{\pi}}^{p*}$.
(5) Use information $\phi^p(\bar{\boldsymbol{\pi}}_k)$, $\mathbf{g}^p(\bar{\boldsymbol{\pi}}_k)$, $\frac{\partial \phi^p}{\partial \bar{\boldsymbol{\pi}}}(\bar{\boldsymbol{\pi}}_k)$, $\frac{\partial \mathbf{g}^p}{\partial \bar{\boldsymbol{\pi}}}(\bar{\boldsymbol{\pi}}_k)$, …, $\phi^p(\bar{\boldsymbol{\pi}}_0)$, $\mathbf{g}^p(\bar{\boldsymbol{\pi}}_0)$, $\frac{\partial \phi^p}{\partial \bar{\boldsymbol{\pi}}}(\bar{\boldsymbol{\pi}}_0)$, $\frac{\partial \mathbf{g}^p}{\partial \bar{\boldsymbol{\pi}}}(\bar{\boldsymbol{\pi}}_0)$ to compute the next *experimental point* $\bar{\boldsymbol{\pi}}_{k+1}$.
(6) Set $k = k + 1$ and repeat Steps 2–5.

Note that Step 2 is experimental and requires estimating plant functions and gradients at each nominal *experimental point* $\bar{\boldsymbol{\pi}}_k$ from measurements $\tilde{\mathbf{y}}^p$ at $\bar{\boldsymbol{\pi}}_k$ and auxiliary *experimental points* $\bar{\boldsymbol{\pi}}_k^1, \ldots, \bar{\boldsymbol{\pi}}_k^{n_\pi}$, while all the other steps are computational. These auxiliary experimental points can be evaluated in parallel if multiple instances of the same experimental system are available. The drawback of this algorithm is that the number of *experimental points* is proportional to the number of iterates of an optimization algorithm, which is typically low but potentially high. This prompts the creation of a slightly different algorithm that takes advantage of the model that is being constructed.

4.3 Hybrid algorithm for experimental design

As mentioned, an alternative is to combine experimental data with the identified model. This results in the following hybrid algorithm to *design the experimental points*:

(1-4) Use Steps 1–4 from the data-driven algorithm.
(5) Use information $\tilde{\mathbf{y}}^p(\bar{\boldsymbol{\pi}}_k^0), \ldots, \tilde{\mathbf{y}}^p(\bar{\boldsymbol{\pi}}_k^{n_\pi}), \ldots, \tilde{\mathbf{y}}^p(\bar{\boldsymbol{\pi}}_0^0), \ldots, \tilde{\mathbf{y}}^p(\bar{\boldsymbol{\pi}}_0^{n_\pi})$ to *identify a model* $\mathbf{y}^m(\bar{\boldsymbol{\pi}})$.
(6) *Adapt the model* $\phi^m(\bar{\boldsymbol{\pi}})$, $\mathbf{g}^m(\bar{\boldsymbol{\pi}})$ given by (13) (with the superscript p replaced by m) such that $\frac{\partial \phi^m}{\partial \bar{\boldsymbol{\pi}}}(\bar{\boldsymbol{\pi}}_k) = \frac{\partial \phi^p}{\partial \bar{\boldsymbol{\pi}}}(\bar{\boldsymbol{\pi}}_k)$, $\mathbf{g}^m(\bar{\boldsymbol{\pi}}_k) = \mathbf{g}^p(\bar{\boldsymbol{\pi}}_k)$, $\frac{\partial \mathbf{g}_a^m}{\partial \bar{\boldsymbol{\pi}}}(\bar{\boldsymbol{\pi}}_k) = \frac{\partial \mathbf{g}_a^p}{\partial \bar{\boldsymbol{\pi}}}(\bar{\boldsymbol{\pi}}_k)$, by adding zeroth-order and first-order modifiers as in

$$\phi^m(\bar{\boldsymbol{\pi}}) = \phi\big(\bar{\mathbf{y}}^m(\bar{\boldsymbol{\pi}}), \bar{\boldsymbol{\pi}}\big) + \boldsymbol{\lambda}_k^\phi \left(\bar{\boldsymbol{\pi}} - \bar{\boldsymbol{\pi}}_k\right), \quad (16a)$$

$$\mathbf{g}^m(\bar{\boldsymbol{\pi}}) = \mathbf{g}\big(\bar{\mathbf{y}}^m(\bar{\boldsymbol{\pi}}), \bar{\boldsymbol{\pi}}\big) + \boldsymbol{\varepsilon}_k^{\mathbf{g}} + \boldsymbol{\Lambda}_k^{\mathbf{g}} \left(\bar{\boldsymbol{\pi}} - \bar{\boldsymbol{\pi}}_k\right), \quad (16b)$$

where $\boldsymbol{\lambda}_k^\phi := \frac{\partial \phi^p}{\partial \bar{\boldsymbol{\pi}}}(\bar{\boldsymbol{\pi}}_k) - \frac{\partial \phi}{\partial \bar{\mathbf{y}}}\big(\bar{\mathbf{y}}^m(\bar{\boldsymbol{\pi}}_k), \bar{\boldsymbol{\pi}}_k\big) \frac{\partial \bar{\mathbf{y}}^m}{\partial \bar{\boldsymbol{\pi}}}(\bar{\boldsymbol{\pi}}_k) - \frac{\partial \phi}{\partial \bar{\boldsymbol{\pi}}}\big(\bar{\mathbf{y}}^m(\bar{\boldsymbol{\pi}}_k), \bar{\boldsymbol{\pi}}_k\big)$, $\boldsymbol{\varepsilon}_k^{\mathbf{g}} := \mathbf{g}^p(\bar{\boldsymbol{\pi}}_k) - \mathbf{g}\big(\bar{\mathbf{y}}^m(\bar{\boldsymbol{\pi}}_k), \bar{\boldsymbol{\pi}}_k\big)$, and $\boldsymbol{\Lambda}_k^{\mathbf{g}} := \frac{\partial \mathbf{g}^p}{\partial \bar{\boldsymbol{\pi}}}(\bar{\boldsymbol{\pi}}_k) - \frac{\partial \mathbf{g}}{\partial \bar{\mathbf{y}}}\big(\bar{\mathbf{y}}^m(\bar{\boldsymbol{\pi}}_k), \bar{\boldsymbol{\pi}}_k\big) \frac{\partial \bar{\mathbf{y}}^m}{\partial \bar{\boldsymbol{\pi}}}(\bar{\boldsymbol{\pi}}_k) - \frac{\partial \mathbf{g}}{\partial \bar{\boldsymbol{\pi}}}\big(\bar{\mathbf{y}}^m(\bar{\boldsymbol{\pi}}_k), \bar{\boldsymbol{\pi}}_k\big)$.
(7) Compute the next *experimental point* $\bar{\boldsymbol{\pi}}_{k+1}$ as a solution to the problem $\max_{\bar{\boldsymbol{\pi}}} \phi^m(\bar{\boldsymbol{\pi}})$ s.t. $\mathbf{g}^m(\bar{\boldsymbol{\pi}}) \leq \mathbf{0}_g$.
(8) Set $k = k + 1$ and repeat Steps 2–7.

By using this algorithm, the number of *experimental points* may decrease if good models are constructed.

Note that, without Step 6, it would be theoretically possible that the model identified after Step 5 indicated that the optimizer $\bar{\boldsymbol{\pi}}_{k+1}$ in Step 7 is the same experimental point as $\bar{\boldsymbol{\pi}}_k$, which should not happen since Step 4 guarantees that $\bar{\boldsymbol{\pi}}_k$ is not located near $\bar{\boldsymbol{\pi}}^{p*}$. Hence, Step 6 is needed to ensure that, if it was verified in Step 4 that $\bar{\boldsymbol{\pi}}_k$ does not satisfy the KKT conditions for the plant, then $\bar{\boldsymbol{\pi}}_k$ does not satisfy the KKT conditions for the model in Step 7 and the algorithm does not stay at the same experimental point.

These algorithms for experimental design are related to methods for closed-loop evolutionary optimization, where the goal is to use experimental measurements for optimization in a way that exploits the model (Knowles, 2009). Furthermore, one can also note that the data-driven and hybrid algorithms for experimental design are related to some iterative approaches for process optimization, namely, extremum-seeking control and modifier adaptation, respectively (Krstić and Wang, 2000; Marchetti et al., 2009). However, the latter approaches focus on optimization of the

process itself, whereas the focus of the current study is the design of experiments for model identification in a lab-scale system, knowing that this model is then used as a starting point for optimization of the corresponding process.

4.4 Simulation example

In this section, a simulation testbed is used to compare the proposed data-driven and hybrid algorithms and assess the number of experimental points. This simulation testbed corresponds to a slightly modified version of the bioreactor model presented by Nolan and Lee (2011). This bioreactor model includes $R = 34$ reactions and $S = 39$ species, from which $S_{ic} = 24$ are intracellular and $S_{ec} = 15$ are extracellular. The outputs $\mathbf{y}(t)$ correspond to the concentrations $\mathbf{c}_a(t)$ of $S_a = 13$ measured extracellular species.

The kinetic expressions and corresponding kinetic parameters are given by Nolan and Lee (2011) for some reactions. These postulated kinetic expressions are denoted as $\mathbf{p}(t)$ and depend on the concentrations of measured extracellular species except the ones of biomass $c_{biom}(t)$ and monoclonal antibodies $c_{\mathrm{mAb}}(t)$. The concentrations of these $S_c = 11$ species, such as Glc (glucose) and Lac (lactose), are denoted as $\mathbf{c}_c(t)$ since they are controlled. More details about this kinetic model are available from the author.

From the generic dynamic model (1) and the fact that the dynamic model given by Nolan and Lee (2011) is such that $\mathbf{N}_{ic}^{\mathrm{T}}\mathbf{r}_c\big(\mathbf{c}(t)\big) = \mathbf{0}_{S_{ic}}$ and $\mathbf{r}_c\big(\mathbf{c}(t)\big) = \mathbf{r}_{vc}\big(\mathbf{c}_c(t)\big)VC(t)$, one can derive the following steady-state model:

$$\mathbf{0}_{S_{ec}} = \mathbf{N}_{ec}^{\mathrm{T}}\mathbf{r}_{vc}\big(\bar{\mathbf{c}}_c\big)\bar{VC} + \bar{\mathbf{C}}_{in}\bar{\boldsymbol{\omega}}_{in} + \bar{\omega}_h\bar{\mathbf{R}}\bar{\mathbf{c}} - \bar{\omega}_p\bar{\mathbf{c}}. \quad (17)$$

For the biomass, we assume that $\bar{\omega}_b = \omega_{dc}\big(\bar{\mathbf{c}}_c\big)\bar{VC}$ for some $\omega_{dc}\big(\bar{\mathbf{c}}_c\big)$, thus $0 = \mathbf{n}_{biom}^{\mathrm{T}}\mathbf{r}_{vc}\big(\bar{\mathbf{c}}_c\big)\bar{VC} - \omega_{dc}\big(\bar{\mathbf{c}}_c\big)\bar{VC}\bar{c}_{biom}$ and

$$\bar{VC} = \tfrac{\mathbf{n}_{biom}^{\mathrm{T}}\mathbf{r}_{vc}(\bar{\mathbf{c}}_c)}{f_{biom}\omega_{dc}(\bar{\mathbf{c}}_c)}. \quad (18)$$

In the remainder, we assume that $\mathbf{R}_c(t) = \mathbf{0}_{S_c\times S_c}$. This implies that the steady state of the controlled outputs $\mathbf{c}_c(t)$ is given by $\mathbf{0}_{S_c} = \mathbf{N}_c^{\mathrm{T}}\mathbf{r}_{vc}\big(\bar{\mathbf{c}}_c\big)\bar{VC} + \bar{\mathbf{C}}_{in,c}\bar{\boldsymbol{\omega}}_{in} - \bar{\omega}_p\bar{\mathbf{c}}_c$, where $\boldsymbol{\omega}_{in}(t)$ are the manipulated inputs. Moreover, we assume that $\omega_p(t)$ is constant with $\bar{\omega}_p = 1\ \mathrm{day}^{-1}$ and there exist as many inputs as controlled outputs, thus control of $\mathbf{c}_c(t)$ with no steady-state error can be implemented as shown in Section 3, which allows stating that $\bar{\mathbf{c}}_c = \bar{\mathbf{c}}_c^s$. Hence, one does not need to consider the transient behavior to know that the inputs $\bar{\boldsymbol{\omega}}_{in}$ are a function of $\bar{\mathbf{c}}_c^s$ given by

$$\bar{\boldsymbol{\omega}}_{in} = \bar{\omega}_p\bar{\mathbf{C}}_{in,c}^{-1}\left(\bar{\mathbf{c}}_c^s - \mathbf{N}_c^{\mathrm{T}}\mathbf{r}_{vc}(\bar{\mathbf{c}}_c^s)\tfrac{\mathbf{n}_{biom}^{\mathrm{T}}\mathbf{r}_{vc}(\bar{\mathbf{c}}_c^s)}{f_{biom}\omega_{dc}(\bar{\mathbf{c}}_c^s)\bar{\omega}_p}\right). \quad (19)$$

Using a similar notation for the case of monoclonal antibodies, it is known that $0 = \mathbf{n}_{\mathrm{mAb}}^{\mathrm{T}}\mathbf{r}_{vc}\big(\bar{\mathbf{c}}_c\big)\bar{VC} - \bar{\omega}_p\bar{c}_{\mathrm{mAb}}$ and

$$\bar{c}_{\mathrm{mAb}} = \mathbf{n}_{\mathrm{mAb}}^{\mathrm{T}}\mathbf{r}_{vc}(\bar{\mathbf{c}}_c^s)\tfrac{\mathbf{n}_{biom}^{\mathrm{T}}\mathbf{r}_{vc}(\bar{\mathbf{c}}_c^s)}{f_{biom}\omega_{dc}(\bar{\mathbf{c}}_c^s)\bar{\omega}_p}. \quad (20)$$

In principle, any values can be freely chosen for the steady-state setpoints $\bar{\mathbf{c}}_c^s$, which makes them an obvious choice as decision variables of the steady-state optimization problem that corresponds to the maximization of $\bar{c}_{\mathrm{mAb}}$ in this example. The only constraint is that the steady-state inputs $\bar{\boldsymbol{\omega}}_{in}$ must be nonnegative since they correspond to inlet rates. If there is a one-to-one correspondence between inlets and species with controlled concentrations, both $\bar{\mathbf{C}}_{in,c}$ and $\bar{\mathbf{C}}_{in,c}^{-1}$ are nonnegative diagonal matrices, which implies that $\bar{\boldsymbol{\omega}}_{in} \geq \mathbf{0}_{S_c}$ if and only if $\bar{\mathbf{c}}_{in,c} = \bar{\omega}_p^{-1}\bar{\mathbf{C}}_{in,c}\bar{\boldsymbol{\omega}}_{in} \geq \mathbf{0}_{S_c}$.

Hence, according to the previous developments, the following steady-state optimization problem is considered:

$$\max_{\bar{\boldsymbol{\pi}}}\ \phi^p(\bar{\boldsymbol{\pi}}) := \mathbf{n}_{\mathrm{mAb}}^{\mathrm{T}}\mathbf{r}_{vc}\big(\bar{\mathbf{c}}_c^s\big)\tfrac{\mathbf{n}_{biom}^{\mathrm{T}}\mathbf{r}_{vc}(\bar{\mathbf{c}}_c^s)}{f_{biom}\omega_{dc}(\bar{\mathbf{c}}_c^s)\bar{\omega}_p}, \quad (21a)$$

$$\text{s.t. } \mathbf{g}^p(\bar{\boldsymbol{\pi}}) := \mathbf{N}_c^{\mathrm{T}}\mathbf{r}_{vc}\big(\bar{\mathbf{c}}_c^s\big)\tfrac{\mathbf{n}_{biom}^{\mathrm{T}}\mathbf{r}_{vc}(\bar{\mathbf{c}}_c^s)}{f_{biom}\omega_{dc}(\bar{\mathbf{c}}_c^s)\bar{\omega}_p} - \bar{\mathbf{c}}_c^s \leq \mathbf{0}_g. \quad (21b)$$

Then one can use the data-driven and hybrid algorithms for experimental design. For better visualization of the results, only 2 degrees of freedom out of the 11 steady-state setpoints $\bar{\mathbf{c}}_c^s$ vary. More precisely, the algorithms vary only the setpoints $\bar{\boldsymbol{\pi}} = (\bar{c}_{\mathrm{Glc}}^s, \bar{c}_{\mathrm{Lac}}^s)$. At each iteration k, the gradients $\frac{\partial\phi^p}{\partial\bar{\boldsymbol{\pi}}}(\bar{\boldsymbol{\pi}}_k)$, $\frac{\partial\mathbf{g}^p}{\partial\bar{\boldsymbol{\pi}}}(\bar{\boldsymbol{\pi}}_k)$ are estimated via finite-difference approximations, which requires $n_\pi = 2$ auxiliary experimental points $\bar{\boldsymbol{\pi}}_k^1$, $\bar{\boldsymbol{\pi}}_k^2$ for each nominal experimental point $\bar{\boldsymbol{\pi}}_k$. The step away from each nominal point to compute the gradient with respect to a decision variable corresponds to 2% of the initial value of that variable. Furthermore, these perturbations are in the direction of smaller $\bar{c}_{\mathrm{Glc}}^s$ and larger $\bar{c}_{\mathrm{Lac}}^s$ because this direction represents a smaller risk of violation of the constraint $-\bar{c}_{in,\mathrm{Lac}} \leq 0$.

It is assumed in this example that the steady-state inputs $\bar{\boldsymbol{\omega}}_{in}^p(\bar{\boldsymbol{\pi}})$ are noise-free since their transient values result from high-frequency feedback control, while the steady-state uncontrolled outputs $\bar{\mathbf{c}}_n^p(\bar{\boldsymbol{\pi}})$ are assumed to be corrupted by additive zero-mean Gaussian noise with a standard deviation of 0.2% of its true value, which can be approximated in practice by taking several replications for each experimental point. Furthermore, it is assumed that each postulated reaction rate at steady state $\bar{p}$ that is modeled by the hybrid algorithm is corrupted by additive zero-mean Gaussian noise with a standard deviation of 0.2% of its true value. Note that the rates $\bar{\mathbf{p}}$ can be computed from the quantities $\bar{VC}$, $\bar{\boldsymbol{\omega}}_{in}$, $\bar{\mathbf{c}}_c$, $\bar{c}_{\mathrm{mAb}}$ by solving the relevant equations.

Figure 1 shows the progress of the data-driven algorithm. This algorithm stops after evaluating 9 nominal experimental points $\bar{\boldsymbol{\pi}}_k$ and 18 auxiliary points $\bar{\boldsymbol{\pi}}_k^1$ or $\bar{\boldsymbol{\pi}}_k^2$, when the cost value is more than 3000 times the predicted cost improvement. Each blue circle represents one of the 27 experimental points, while the red line corresponds to the progress over the iterations. Recall that $n_\pi + 1 = 3$ experimental points are necessary at each iteration to compute the gradients. Hence, most of the blue circles do not coincide with the red line since they correspond to auxiliary points.

Figure 2 shows the progress of the hybrid algorithm. This algorithm stops after evaluating 8 nominal experimental points $\bar{\boldsymbol{\pi}}_k$ and 16 auxiliary points $\bar{\boldsymbol{\pi}}_k^1$ or $\bar{\boldsymbol{\pi}}_k^2$, slightly fewer than the data-driven algorithm. The model identified in Step 5 of the algorithm possesses the structure $\bar{p} = \frac{p_4\bar{c}_{\mathrm{Glc}}+p_5\bar{c}_{\mathrm{Lac}}+p_6\bar{c}_{\mathrm{Glc}}\bar{c}_{\mathrm{Lac}}}{p_1+p_2\bar{c}_{\mathrm{Glc}}+p_3\bar{c}_{\mathrm{Lac}}+\bar{c}_{\mathrm{Glc}}\bar{c}_{\mathrm{Lac}}}$ for each postulated steady-state reaction rate $\bar{p}$, where $p_1, \ldots, p_6$ are unknown parameters. Note that the algorithm evaluates 2 nominal experimental points, labeled 0 and 1 in Figure 2, and 4 other auxiliary experimental points, that is, 6 experimental points in total, before a valid model (with 6 parameters for each rate $\bar{p}$) can be identified, adapted, and used by the hybrid algorithm in Steps 5, 6, and 7. Once such a model is available, the hybrid algorithm follows the correct direction toward the plant optimum, although the identified model is considerably less complex than the true kinetic model.

By using either algorithm, one can measure steady-state attributes, that is, concentrations $\bar{\mathbf{c}}_n$ and $\bar{\mathbf{c}}_{in,c}$, for a number of experimental points that are close to a plant optimum.

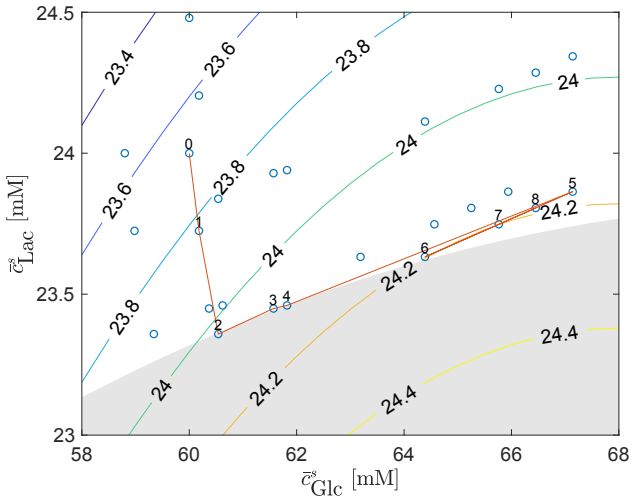

Fig. 1. Evolution of $\bar{c}_{\mathrm{mAb}}$ as a function of $\bar{c}^s_{\mathrm{Glc}}$ and $\bar{c}^s_{\mathrm{Lac}}$ over the iterations of the data-driven algorithm, with the infeasible region represented by the shaded area.

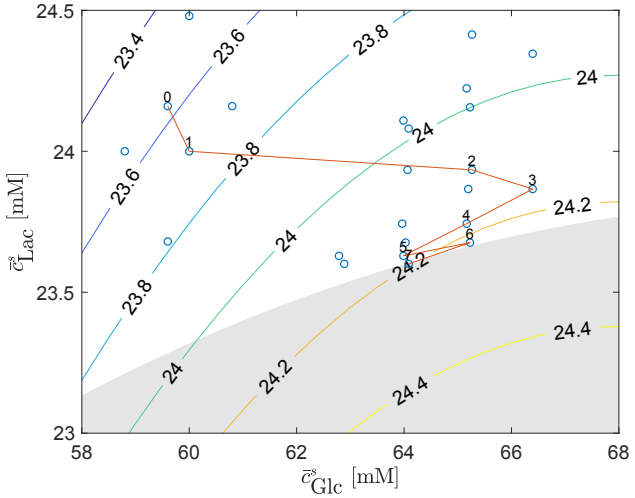

Fig. 2. Evolution of $\bar{c}_{\mathrm{mAb}}$ as a function of $\bar{c}^s_{\mathrm{Glc}}$ and $\bar{c}^s_{\mathrm{Lac}}$ over the iterations of the hybrid algorithm, with the infeasible region represented by the shaded area.

This allows the identification of a model that represents well the plant, that is, the true perfusion bioreactor, in the most interesting region of the space of decision variables.

5. CONCLUSIONS

This paper presented an integrated approach for experimental design, control, and optimization of perfusion bioreactors. The contribution and outlook are outlined below.

The control scheme that was applied in this paper takes advantage of the knowledge about part of the model, is rather simple to tune thanks to the clear meaning of its parameters, converges quickly to its setpoints, and eliminates steady-state error. In future work, it would be interesting to investigate how much one can improve the control performance by using complete models of perfusion bioreactors and other control structures. The different approches may then be tested on a real perfusion bioreactor.

Two algorithms for designing experiments that use the optimality conditions of the experimental system have been presented. One algorithm is purely data-driven, while the other algorithm is a hybrid version that combines experimental data with the identified model. Furthermore, a simulated testbed has been used to compare data-driven and hybrid algorithms and assess the number of experimental points. In future work, it would also be interesting to compare these algorithms to other approaches that optimize criteria related to the Fisher information matrix with respect to their ability to identify a model that can predict well the optimality conditions of perfusion bioreactors.

This paper foresees that the ideal operation of perfusion bioreactors consists in the integration of (i) a control approach with steady-state properties guaranteed via control design and closed-loop stability and performance that can be verified using an approximate dynamic model and (ii) an approach for optimization of steady-state setpoints that takes advantage of a steady-state model obtained via experimental design and model identification techniques designed for this purpose. Hence, the methods in this paper pave the way for rational design of models for perfusion bioreactors that are suited to their reliable and optimal operation.

REFERENCES

Bonvin, D., Georgakis, C., Pantelides, C.C., Barolo, M., Grover, M.A., Rodrigues, D., Schneider, R., and Dochain, D. (2016). Linking models and experiments. *Ind. Eng. Chem. Res.*, 55(25), 6891–6903.

Chotteau, V. (2015). Perfusion processes. In M. Al-Rubeai (ed.), *Animal Cell Culture*, 407–443. Springer.

Clincke, M.F., Mölleryd, C., Samani, P.K., Lindskog, E., Fäldt, E., Walsh, K., and Chotteau, V. (2013). Very high density of Chinese hamster ovary cells in perfusion by alternating tangential flow or tangential flow filtration in WAVE bioreactor™–part II: Applications for antibody production and cryopreservation. *Biotechnol. Prog.*, 29(3), 768–777.

Farschman, C.A., Viswanath, K.P., and Ydstie, B.E. (1998). Process systems and inventory control. *AIChE J.*, 44(8), 1841–1857.

Knowles, J. (2009). Closed-loop evolutionary multiobjective optimization. *IEEE Comput. Intell. M.*, 4(3), 77–91.

Krstić, M. and Wang, H.H. (2000). Stability of extremum seeking feedback for general nonlinear dynamic systems. *Automatica*, 36(4), 595–601.

Marchetti, A., Chachuat, B., and Bonvin, D. (2009). Modifier-adaptation methodology for real-time optimization. *Ind. Eng. Chem. Res.*, 48(13), 6022–6033.

Nolan, R.P. and Lee, K. (2011). Dynamic model of CHO cell metabolism. *Metab. Eng.*, 13(1), 108–124.

Nuñez, S., De Battista, H., Garelli, F., Vignoni, A., and Picó, J. (2013). Second-order sliding mode observer for multiple kinetic rates estimation in bioprocesses. *Control Eng. Practice*, 21(9), 1259–1265.

Pollock, J., Ho, S.V., and Farid, S.S. (2013). Fed-batch and perfusion culture processes: Economic, environmental, and operational feasibility under uncertainty. *Biotechnol. Bioeng.*, 110(1), 206–219.

Rodrigues, D., Amrhein, M., Billeter, J., and Bonvin, D. (2018). Fast estimation of plant steady state for imperfectly known dynamic systems, with application to real-time optimization. *Ind. Eng. Chem. Res.*, 57(10), 3699–3716.

Rodrigues, D. and Hjalmarsson, H. (2019). Stability and performance analysis of control based on incomplete models. *IFAC-PapersOnLine*, 52(1), 874–879.